Cohesive-Length Scales for Damage and Toughening Mechanisms

R. B. Sills[*] and M. D. Thouless[§]

[*]*Sandia National Laboratories*
Livermore, CA 94550 USA

[§]*Department of Mechanical Engineering*
Department of Materials Science & Engineering
University of Michigan
Ann Arbor, MI 48109-2125, USA

Abstract

While toughening and damage might seem to be two contradictory concepts for the mechanics of crack growth, they are actually the same phenomena perceived from two different vantage points. Similarly, the concepts of extrinsic and intrinsic toughening, defined in terms of whether a toughening mechanism occurs behind or ahead of a crack, depend on the definition of a crack tip that, in the absence of a singularity, can be somewhat arbitrary. Cohesive-zone models provide useful numerical tools for rationalizing these different concepts and, here, we use them to show how different perspectives of toughening and damage can be understood.

The concept of a cohesive length, defined in terms of an effective modulus and the magnitudes of the local tractions and displacements (or work done), can be generalized so that it can be used at any load before failure, and at any point along the interface. We show that this general concept allows multiple damage and toughening mechanisms, each with its own characteristic cohesive length, to be described and tracked in terms of a single traction-separation law. In general, the onset of damage corresponds to an increase in cohesive length. This tends to weaken a material unless compensated for by a sufficiently high increment of additional toughness. The ratio between the cohesive length of a particular damage / toughening mechanism and any relevant geometrical length determines whether the mechanism needs to be included in the cohesive-zone formulation. Furthermore, it appears that diffuse damage and crack jumping between interfaces may be induced when the cohesive length of a damage mechanism is large compared to a micro-structural length. It is speculated that this may be of some relevance to the design of hierarchical materials.

(December 7, 2013)
(Revised: May 27, 2014)

1. Introduction

Toughening mechanisms can be categorized into two types: *intrinsic* and *extrinsic* (Fig. 1) [Ritchie, 2011]. Intrinsic mechanisms are the dissipative processes that occur ahead of the crack tip in what is known as a crack-tip process zone. Extrinsic mechanisms are those that occur behind the crack tip. Examples of intrinsic toughening include plasticity, void growth, micro-cracking, phase changes and crazing. Examples of extrinsic toughening include bridging zones and the unloading of a crack-tip process zone as it passes into the wake of a crack. However, as will be emphasized in this work, the physical reality that singular stresses do not occur in real materials means that the location of a crack tip can be arbitrarily defined, and the division of toughening mechanisms into intrinsic and extrinsic is a matter of perspective and convenience. For example, the crack tip could be defined as being the point at which there is no interaction between the crack surfaces. In this case, all deformation up to the point of rupture would be associated with intrinsic toughening. Alternatively, the crack tip could be defined as being the point at which one deformation process ceases; for example, the point at which the matrix material ruptures leaving bridging fibers as the only interaction between the crack surfaces. Any mechanism acting ahead of this point would then be associated with intrinsic toughening; any mechanism acting behind would be associated with extrinsic toughening.

Recognition of the arbitrary nature of the definition of a crack tip is important because understanding the processes by which one might strengthen a material can be influenced by one's perception of the nature of the toughening. Furthermore, it should be recognized that intrinsic toughening mechanisms that introduce an aspect of non-

linearity into the crack-tip process zone ahead of a crack could equally-well be viewed as damage mechanisms that might be perceived to weaken a material [Thouless 1988]. Indeed, the question of whether damage (intrinsic-toughening) mechanisms strengthen or weaken a material is addressed in this paper.

Cohesive-zone models provide useful analytical tools for exploring the concepts of toughening and damage (Fig.1). Traction-separation laws, which dictate the tractions across a crack plane as a function of separation distance, can be used as a means of representing various forms of crack-tip processes into a finite-element analysis that allows crack propagation to evolve naturally upon loading. Numerical experiments can be performed in which the stress evolution, crack propagation and applied loads are investigated for different forms of cohesive laws, and the results can be interpreted from different perspectives of toughening, and with different definitions of the crack tip. Since the behavior of the body from a global perspective has to be independent of any perspective chosen to describe the mechanics (Fig. 1), this approach provides a means to rationalize different perceptions of toughening under unifying concepts.

The concept of a cohesive, fracture, or bridging length has been established for composites and other materials [Hillerborg *et al*., 1976; Bao and Suo, 1992]. For mode-I, this length is dependent on three important parameters: (i) the cohesive or bridging strength, $\hat{\sigma}$, which is the maximum stress that can be supported by any element of material in the crack plane; (ii) the mode-I toughness, Γ_I, which is the total energy dissipated by creating unit area of new crack surface, including fracture of any ligaments across the crack plane; and (iii) the effective modulus of the material on either side of the interface, $\overline{E}^*$. These three quantities can be combined to give a material parameter

with dimensions of length, so that a nominal mode-I fracture length can be defined as [Hillerborg *et al*., 1976; Bao and Suo, 1992; Sills and Thouless, 2013]

$$\zeta_I = \frac{\overline{E}^* \Gamma_I}{\hat{\sigma}^2}, \tag{1a}$$

where the effective modulus for a bi-material system is

$$\overline{E}^* = \frac{2\overline{E}_1\overline{E}_2}{\overline{E}_1 + \overline{E}_2} \ , \tag{1b}$$

$\overline{E}$ is Young's modulus (E in plane stress, $E/(1-\nu^2)$ in plane strain, and ν is Poisson's ratio), and the subscripts 1 and 2 refer to the materials on either side of the interface.

The ratio of the nominal fracture length to the smallest geometrical dimension associated with fracture, such as the crack length, a, the uncracked ligament length, L, or the laminate thickness, h, gives a non-dimensional nominal fracture-length scale. If this fracture-length scale is small, less than about 0.4[1], crack growth is controlled by the toughness. An energy-release rate based on linear-elasticity can be calculated and compared to the interfacial toughness to determine if the crack will grow. As will be discussed later, this gives an upper-bound for the strength of a bonded system. If the fracture-length scale is large, greater than about 2, crack growth is controlled by the cohesive strength [Parmigiani & Thouless, 2007]. This provides a second upper-bound for the strength of a bonded system that can be obtained by equating the average stress supported by the interface to its cohesive strength. At intermediate scales, there is a smooth transition between toughness- and strength-controlled fracture. The two limits are linked to the concepts of notch sensitivity and insensitivity [Bao and Suo, 1992].

[1] This value of 0.4 has been selected to make a connection to the common definition for the validity of linear-elastic fracture mechanics.

When failure is controlled by toughness, the strength of the material is sensitive to geometrical stress concentrations, such as cracks or changes in section. When failure is controlled by cohesive strength, geometrical features do not concentrate stresses, leaving the strength to be dictated by the average stress on the smallest load-bearing ligament.

In a companion paper [Sills and Thouless, 2013], it was observed that an instantaneous cohesive length, defined in terms of the displacement and work done by the cohesive tractions, can be defined for any increment of loading up to, and including, the point of fracture. The definition of the instantaneous cohesive length can be illustrated by reference to a generic form of the mode-I traction-separation law that will be used in this paper (Fig. 2). When the instantaneous displacement from the equilibrium separation of the interface is δ_n, the cohesive tractions have done work $\mathcal{W}_I$. The mode-I instantaneous cohesive length is then defined as

$$\xi_I = \frac{\overline{E}^* \delta_n^2}{\mathcal{W}_I} = \frac{\overline{E}^* \mathcal{W}_I}{\sigma_{avg}^2} \quad , \tag{2}$$

where σ_{avg} is the average stress exerted by the cohesive element up to the displacement of interest. An instantaneous cohesive-length scale can then be defined by comparing the magnitude of ξ_I to a characteristic dimension, such as a crack size, ligament length, kink length or microstructural length.

The parameters at the tip of the cohesive crack, defined as the last location along a crack surface at which tractions occur (Fig, 1), are designated by the subscript "*o*", so that the work done by the mode-I cohesive tractions is denoted by $\mathcal{W}_{Io}$, and the corresponding instantaneous cohesive length is denoted by ξ_{Io}. When fracture occurs in pure mode-I, $\mathcal{W}_{Io} = \Gamma_I$, and the instantaneous cohesive length at fracture is directly

related to the nominal fracture length, ζ_I, through a numerical constant related to the shape of the traction-separation law. It should be noted that ξ_o scales with the lengths of features in the stress field ahead of a cohesive crack, which might be used as measures of a cohesive-zone length. However, the precise relationship depends on the definition of the cohesive-zone length and on the shape of the traction-separation law.

The concept of an instantaneous cohesive length can be used at arbitrary positions along an interface, not just at the cohesive crack tip. This allows different portions of a single cohesive law to be used to describe multiple damage / toughening mechanisms, each having their own instantaneous cohesive length, measured from the displacement at which the mechanism was triggered. For example, the initial portion ($\delta_n < \delta_{n1}$) of the cohesive law shown in Fig. 2 (which could be considered to represent matrix cracking in a composite) will have a much smaller value of ξ_I than the subsequent portions of the law corresponding to damage or bridging mechanisms.

The concepts of nominal fracture length and instantaneous cohesive length can also be extended to mode-II. Mixed-mode and modulus-mismatch effects have been discussed elsewhere [Sills and Thouless, 2013]. For simplicity, such effects are not considered in this paper, and the subscripts "I" and "II" will be dropped. Furthermore, in this paper bi-material systems will not be considered, so the effective modulus is designated simply by $\overline{E}$.

In this paper, different shapes of traction-separation laws, representing different types of damage / toughening mechanisms are incorporated into cohesive-zone models. The results are analyzed from the perspectives of intrinsic toughening, extrinsic

toughening and damage, and the effects of cohesive-length scales on stress fields and the strength of interfaces are examined. Two additional points are made about cohesive-length scales. The first point is to emphasize the importance of appropriately matching the geometrical lengths to cohesive lengths in any experiment designed to extract cohesive parameters. The second point is to demonstrate a possible relationship between cohesive lengths and micro-structural lengths in the generation of diffuse damage that is an important aspect of many toughening mechanisms.

2. Approach

2.1 Implementation of cohesive-zone and traction-separation law

The cohesive zone model developed by Yang *et al*. [1999] was utilized for all results presented in this work. It was implemented by means of a user-defined element (UEL) in ABAQUS v6.9. All simulations were run using three- and four-node linear, fully-integrated, plane-strain, continuum elements. Loads were applied with a displacement boundary condition and stress uniformity along the boundary was confirmed for each simulation to ensure a far-field constant stress was well represented. Symmetry boundary conditions were applied along the vertical and horizontal centerlines of the specimen where appropriate (unless shown otherwise). Mesh-refinement sufficiency was verified iteratively and by comparison with analytical solutions. For problems with crack growth, mesh refinement is required along the entire domain over which the crack extends. It was found that interfacial stresses are sufficiently resolved provided the cohesive-element length, l_e, is less than about 0.02ξ (a similar requirement would also be put on mode-II calculations). This requirement has ramifications for problems in which ξ varies ahead of a crack, and it should be emphasized that this means the necessary

extent of mesh refinement is dictated by the traction-separation law shape (since this sets ξ). The cohesive-zone half-thickness was set at $h_{cz}/a = 1.11\text{x}10^{-4}$ so that elements had a reasonable aspect ratio. A sample mesh is pictured in Fig. 3. The deformations associated with two distinct portions of a cohesive law such as that shown in Fig. 2 can be clearly identified. This figure illustrates the two definitions of a crack tip identified in Fig. 1: (i) the unbridged or cohesive-zone crack tip, behind which there are no tractions and (ii) the matrix-crack tip.

The 4-part law shown in Fig. 2 is a generalized form of a traction-separation law that provides an approximate model for matrix cracking and bridging in a composite. Cohesive-zone models have been extensively studied in the context of composite materials under both mode-I and mixed-mode conditions [Sorensen and Jacobsen, 1998; Li *et al.*, 2005; Sorensen and Jacobsen, 2009]. The cohesive law presented in Fig. 2 follows the concept first discussed by Cox and Marshall [1994] that it can be used to represent both matrix cracking and bridging in a composite. This 4-part law is the most general form of some simple cases that are often used as generic traction-separation laws: linear-hardening (Fig. 4a); linear-softening (Fig 4b); constant-stress (Fig. 4c); and trapezoidal (Fig. 4d). As observed in Sills and Thouless [2013], the linear-hardening law is particularly interesting because the instantaneous cohesive length is constant. Therefore, it incorporates no concept of damage, and provides a prototypical cohesive law against which the specific effects of damage can be compared. For example, the other three simple laws shown in Fig. 4 reach a limiting cohesive strength *before* failure, which can be equated to the onset of damage (or bridging). In the context of using these simple laws to describe a composite, this initial portion of the traction-separation law

will be associated with matrix cracking[2], or intrinsic toughening, and the latter parts of the curve will be associated with bridging, extrinsic toughening, or damage.

2.2 Intrinsic and extrinsic toughening

The distinctions between extrinsic toughness, intrinsic toughness / damage, matrix-crack tips, and cohesive-zone crack tips are illustrated by means of the mode-I center-cracked geometry shown in Fig. 5. The model has a cohesive interface running along the crack plane all the way to the specimen boundaries. The mode-I cohesive law shown in Fig. 2 applies along the whole length of the interface; there is no embedded elastic crack tip where stresses could be unbounded. The width of the specimen is $2b$, the unbridged crack length is $2a_o$, and the distance ahead of the unbridged, or cohesive, crack tip is r. The displacements on the boundaries are such that the remote applied stress is σ^∞.

From the perspective of intrinsic toughening or damage, the nominal energy-release rate for this geometry with respect to the crack tip can be calculated from linear-elastic fracture mechanics (LEFM) [Tada *et al.*, 1985]

$$\mathcal{G}_o^\infty = \pi f\left(a_o/b\right)\frac{\sigma^{\infty 2} a_o}{\bar{E}} \tag{4}$$

where,

$$f\left(a_o/b\right) = \frac{\left[1-0.5\left(a_o/b\right)+0.326\left(a_o/b\right)^2\right]^2}{\left(1-a_o/b\right)}$$

The superscript "∞" is used to denote the nominal energy-release rate calculated from linear-elasticity, corresponding to a cohesive-length scale identically equal to zero. The subscript "o" is used to denote the fact that the energy-release rate is calculated with

[2] An infinite steepness for the initial portion of the traction-separation laws would correspond to a matrix with no toughness, and an instantaneous cohesive length $\xi = 0$.

respect to the unbridged or cohesive-zone crack tip. The singular stress field ahead of the crack tip corresponding to the LEFM solution is given by

$$\frac{\sigma}{\sigma^{\infty}} = \sqrt{\frac{f\left(a_o/b\right)}{2}}\left(\frac{r}{a_o}\right)^{-1/2} \quad . \tag{5}$$

At the heart of LEFM approaches to problems involving intrinsic toughening or damage is the notion that for small cohesive lengths there is a portion of the stress field ahead of the crack that can still be described by the inverse square-root form of Eqn. (5). In this context, it should be noted that the nominal energy-release rate has been defined in Eqn. (4) in terms of the remote stress, effective modulus and geometry, so that it has meaning even when the conditions of LEFM are not satisfied, and it does not represent the actual energy-release at the crack tip.

From the perspective of extrinsic toughening, one can arbitrarily define the location of the crack tip according to what portion of the cohesive law one wishes to designate as representing an extrinsic toughening mechanism. For the purposes of this paper, we will define the intrinsic (or matrix) crack tip as being the point on the interface where the traction-separation law has reached δ_{n1} (Fig. 2). This corresponds to a crack tip at a distance Δa ahead of the cohesive crack tip, so the new crack length is

$$a_m = a_o + \Delta a \, . \tag{6}$$

The intrinsic (or matrix) toughness is given by

$$\Gamma_m = \hat{\sigma}_1 \delta_1 / 2 , \tag{7}$$

while the extrinsic toughness, Γ_b, is

$$\Gamma_b = \mathcal{W}_o - \Gamma_m \, . \tag{8}$$

Under LEFM conditions, the remote energy-release rate can be calculated in terms of the

matrix-crack length, a_m, and the applied stress as

$$\mathcal{G}_m^{\infty} = \pi f\left(a/b\right)\frac{\sigma^{\infty 2} a}{\bar{E}} \tag{9}$$

The subscript "*m*" is used to denote the fact that the energy-release rate is calculated with respect to the matrix crack tip. The value of this energy-release rate required to propagate the matrix crack is considered to be the toughness of the composite, and a plot of how it varies with crack extension, Δa, is known as an *R*-curve.

The stress field predicted by LEFM at the tip of a propagating matrix crack is given by

$$\frac{\sigma\sqrt{a_o}}{\sqrt{\bar{E}\Gamma_m}} = \frac{1}{\sqrt{2\pi}}\left(\frac{r-\Delta a}{a_o}\right)^{-1/2} \tag{10}$$

where *r* is measured from the original cohesive crack tip. A comparison between Eqns. (10) and (5) emphasizes that an inverse square root singularity should be expected for the stress field ahead of a crack whether it is measured from the cohesive crack tip or from the matrix crack tip. The validity of such an expectation is one of the issues that will be examined in the analyses that follow.

3. Intrinsic toughening / damage

3.1. Stress field for linear-hardening law

A linear-hardening traction-separation law (Fig. 4a) has the form

$$\sigma = k\delta, \tag{11}$$

Therefore, the instantaneous cohesive length is constant throughout the entire loading history and at any location along the interface. It can be expressed as

$$\xi = 2\bar{E}/k. \tag{12}$$

Figure 6 shows plots of the stress field ahead of the cohesive crack tip for different

levels of ξ. As expected, these plots do not change during loading since the instantaneous cohesive-length scale is a constant. For the lower values of ξ, there is a region where the stresses are approximately described by the LEFM expression of Eqn. (5), but slightly elevated above that level. The stresses deviate significantly from this relationship and exhibit a plateau close to the crack tip. It should be noted that this plateau is completely unrelated to any concept of cohesive strength, because the stress in a linear-hardening law is not limited (except at the point of failure). Rather, recognizing that $\mathcal{W} = \sigma^2/2k$, Eqn. (12) can be used to show that the stress is given by

$$\sigma = 2\left(\frac{\bar{E}\mathcal{W}}{a_o}\right)^{1/2}\left(\frac{\xi}{a_o}\right)^{-1/2}. \tag{13a}$$

As ξ becomes very small, the work done by the tractions at the crack tip, $\mathcal{W}_o$, approaches $\mathcal{G}_o^{\infty}$. Using Eqn. (4), it is then possible to show that the stresses at the crack tip must be given by

$$\frac{\sigma_o}{\sigma^{\infty}} = 2\sqrt{\pi f\left(a_o/b\right)}\left(\frac{\xi}{a_o}\right)^{-1/2} \tag{13b}$$

3.2. Stress field for cohesive laws with damage

The other laws considered in this paper have a cohesive strength that is reached before (rather than simultaneously with) failure of the element. Therefore, the cohesive strength at the crack tip will limit the stresses prior to failure. This cohesive strength can be considered to represent either the onset of damage (intrinsic toughening) ahead of the crack, or the propagation of a matrix crack leaving a wake of extrinsic toughening behind it. The commonly used laws of Figs. 4(b), (c) and (d) represent simple cases where the peak stress for damage or bridging is identical to the strength of the matrix

crack. In the numerical examples that follow, finite, but steep, initial loading slopes were assumed, (δ_1/δ_c = 0.001 for the linear-softening and constant-stress laws; δ_1/δ_c = 0.01 for the trapezoidal law), with the matrix toughness being only 0.05% of the overall toughness for the constant-stress law, 0.1% for the linear-softening law, and 0.7% for the trapezoidal law. These initial slopes correspond to instantaneous cohesive-length scales of ξ_o/a_o = 0.0020 for the first two laws and 0.0268 for the trapezoidal law. An additional example using a more involved cohesive law that represents matrix cracking followed by fiber bridging was also used. For this example, $\delta_1/\delta_c = 0.0999$, $\delta_2/\delta_c = 0.1$, $\hat{\sigma}_1/\hat{\sigma}_2 = 10$, $\hat{\sigma}_1/\hat{\sigma}_3 = 6$, with an initial instantaneous cohesive-length scale of $\xi_o/a_o = 0.0040$ For the trapezoidal law $\delta_3/\delta_c = 0.5$, but for all other laws used in this paper $\delta_3/\delta_c = 0.999$.

Plots of how the stresses along the interface evolve during loading (Fig. 7) show similar features to those of Fig. 6. However, close to the crack tip, the magnitude of the stresses has an additional limitation imposed by the cohesive strength (represented by the cusp in the stress plots). As will be discussed in the subsequent section, the location of this cusp can be taken to be the position of the matrix crack; its progression across the specimen during loading can be seen in the plots of Fig. 7. As with the linear-hardening law, there is a region outside the damage / toughening zone where the stresses follow an inverse square-root relationship for values of ξ_o/a_o less than about 1, and are elevated above the LEFM level.

3.3. Damage or intrinsic toughening?

As shown in Fig. 8a, the elevation of the stresses in the inverse-square-root

regime is also reflected in the observation that $\mathcal{W}_o$ is elevated over $\mathcal{G}_o^\infty$ for non-zero values of ξ_o. As can be seen from this figure, the ratio of $\mathcal{W}_o/\mathcal{G}_o^\infty$ increases with ξ_o/a_o, and is elevated by about 10% for a value of $\xi_o/a_o \approx 0.4$. Plots for different cohesive-laws show similar, but not identical,[3] behavior.

The significance of this relationship between ξ_o/a_o and $\mathcal{W}_o/\mathcal{G}_o^\infty$ can be seen by considering what happens if one were to change various geometrical or material/interfacial parameters. For example, if one were to halve the crack length (keeping the ratio *a/b* constant), so as to double ξ_o/a, the stress required to give the same value of $\mathcal{W}_o$ would increase by less than the factor $\sqrt{2}$ predicted by LEFM. Therefore, the condition for fracture would be met at a lower stress than would be expected. A similar argument would apply for doubling the toughness. Owing to the corresponding increase in ξ_o/a_o, the increase in strength would not increase by as much as the increase in toughness would indicate from an LEFM perspective. If the cohesive strength were dropped, the strength of the bonded system could only be maintained if the toughness were increased to compensate for the increase in ξ_o/a. Furthermore, the elevation of $\mathcal{W}_o$ over $\mathcal{G}_o^\infty$ means that the calculation of a strength based on LEFM will always be an upper bound for any non-zero value of ξ_o. This is shown in the plot of Fig. 8b, in which the strength of a cracked interface has been presented as a function of the instantaneous cohesive-length scale at fracture.

Any introduction of damage ahead of a crack that causes ξ_o to increase without

[3] It is not apparent whether there is an alternative definition of instantaneous cohesive length that would make this relationship independent of cohesive law. A similar issue was raised for mixed-mode problems in Sills and Thouless [2013].

increasing Γ sufficiently to overcome the effect of a larger cohesive-length scale, will always make an interface weaker. It truly is *damage*, even if Γ is increased! If one is designing the traction-separation law of an interface to toughen a material, one must always ensure that any increase in Γ more than off-sets the effect of any increase in ξ_o. For example, one might wish to trigger an additional toughening mechanism such as crazing, void growth or delamination. This could be done by triggering a new damage mechanism at a lower level of interfacial traction than the original cohesive strength (Fig. 9). The new mechanism would be beneficial as a toughening mechanism only if the critical displacement for crack propagation of the new mechanism is large enough to elevate the toughness sufficiently to overcome the increased value of ξ_o (which increases owing to both the decreased cohesive strength and the increased toughness).

4. Extrinsic toughening

As discussed in Section 2.2, the concept of damage (or intrinsic toughening) ahead a crack tip can also be viewed through the lens of extrinsic toughening behind a crack tip, if the definition of the crack tip is moved from the point at which cohesive tractions cease to some intermediate point within the cohesive law. While there is complete flexibility about the definition of a crack tip within this framework, we will define it as the point at which the instantaneous cohesive-length scale begins to change. The point along the interface at which this occurs will be described as the matrix crack tip; the instantaneous cohesive length with respect to the matrix crack will be identified as ξ_m; and the area under the traction-separation curve up to this point will be described as the matrix toughness, Γ_m.

The propagation of the matrix crack across the sample can be monitored from the numerical simulations. An example of matrix-crack growth as a function of applied load is shown in Fig. 10a. In the simulation with a constant-stress law and $\zeta/a_o = 5$, the matrix crack reached the specimen boundary, leaving a fully-bridged crack. In the other simulations, the fracture became unstable before the matrix crack reached the specimen boundary, either because a steady-state crack had evolved (bridging model), or because the stored energy was sufficient for crack growth with no further increase in applied displacement [Li *et al.*, 2005].

At low values of the instantaneous cohesive-length scales, matrix-crack growth can be viewed through the lens of *R*-curve behavior. The data from Fig. 10a can be used to compute *R*-curves for these interfaces, as would be done in an experimental investigation of extrinsic toughening. Such *R*-curves are shown in Fig. 10b. These plots show $\mathcal{G}_m^\infty/\Gamma_m$ against crack growth, $\Delta a/L$, where $\mathcal{G}_m^\infty$ is defined in terms of the matrix crack length and the applied stress (Eqn. 9). Superimposed on this figure are plots of $\mathcal{W}_o/\Gamma_m$ against crack growth, where (from Eqn. 8), $\mathcal{W}_o = \Gamma_m+\Gamma_b$.

It was shown earlier that from an intrinsic-toughening perspective, $\mathcal{W}_o/\mathcal{G}_o^\infty > 1$, with the ratio increasing with cohesive-length scale. Therefore, using a failure criterion of $\mathcal{G}_o^\infty = \Gamma$ provides an over-estimate of the fracture strength. Conversely, Fig. 10b shows that, from an extrinsic-toughening perspective, $\mathcal{W}_o/\mathcal{G}_m^\infty < 1$, with the ratio decreasing with increased toughening. Therefore, the use of an *R*-curve to equate $\mathcal{G}_m^\infty$ to $\Gamma_b + \Gamma_m$ provides an under-estimate of the toughening associated with bridging. The discrepancy increases as the intrinsic cohesive-length scale increases, as it generally

does during the growth of a matrix crack.

When developed from an LEFM perspective, extrinsic crack-growth models assume that there is a stress field with an inverse-square root singularity with respect to the distance from the matrix-crack tip (Eqn. 10). We have already demonstrated the existence of an inverse square-root field for intrinsic toughening (Fig. 7). Since toughening mechanisms that occur within the plane of a crack can be viewed equally from an intrinsic or extrinsic perspective, there is an implication that stress fields should have square-root singular regions whether measured from the cohesive- or matrix-crack tip. To investigate whether this notion is valid, the data from Fig. 7a and 7d (in which stresses are plotted in terms of distance from the cohesive-crack tip) were re-plotted in Figs. 11a and 11b, in terms of distance from the matrix-crack tip.

As can be seen from these figures, there is evidence of an inverse square-root field from both perspectives, but only when the extrinsic / bridging contribution to the toughness is relatively small. These, and related calculations, reveal that the stress field exhibits a singular behavior over a range of distances from the matrix crack tip. However, the singular behavior is generally less strong that an inverse square-root, and only approaches that limit when there is very little extrinsic toughening. In particular, in cases where ξ_o/a_o is relatively small, and there is a square-root singular field from the perspective of the cohesive crack tip, the extrinsic toughening may be too great for such a field to be exhibited from a matrix-crack perspective. The difficulty of maintaining a singular LEFM field from a matrix-crack perspective would seem to raise some concern about the use of stress-intensity factors for crack bridging, although concepts such as *R*-curves do seem to reasonably robust in the limit of small-scale cohesive lengths.

5. Cohesive scales for toughening mechanisms

The concept of an instantaneous cohesive length has been introduced as a way to characterize the development of a cohesive zone, and as a way to describe different toughening / damage mechanisms that may be operating at the tip of a crack. One obvious question that arises is whether there are any implications in comparing the cohesive lengths of different mechanisms to the size of geometrical and microstructural features. Both of these aspects are discussed below.

5.1 Geometrical features

The first case considered is prompted by the experimental observations of Li *et al.* [2005]: a cohesive law developed from observations made on composite specimens with large-scale cracks failed to describe the behavior of uncracked composites. An initial high-strength portion of the law had to be assumed. A model system used to revisit the observations, and to study the interaction between different damage mechanisms and geometrical length scales, is provided by a specific cohesive law of the form shown in Fig. 2. The law chosen had a high matrix-cracking stress ($\hat{\sigma}_1/\hat{\sigma}_2 = 3$, $\xi_m = 0.0024$, $\delta_1/\delta_c = 0.05$, $\delta_2/\delta_c = 0.06$), and a softening phase to represent fiber bridging ($\delta_3 = \delta_c$).

Figure 12 shows an example of how the strength of such a composite varies with crack length. As expected, the matrix strength controls the behavior at very small crack lengths, while the bridging toughness controls the behavior at very long crack lengths. Superimposed on this plot are lines indicating how the cohesive lengths of the two mechanisms compare with the crack length (which is the controlling dimension, since it is always smaller than the ligament length in the plot). In addition, predictions of the strength based on the cohesive-law of each of the two mechanisms considered in

isolation are shown. If the crack length is comparable to the bridging cohesive length, then the bridging law alone is adequate to describe the fracture process. Conversely, once the crack is significantly smaller than the matrix cohesive length, then only the matrix law is needed.

The concept that the cohesive length of a toughening mechanism indicates the geometrical scale at which it needs to be included in a model is probably a general one. For modeling purposes, one needs a cohesive law that matches the scale of the problem being investigated. If one is not interested in how a composite behaves in the presence of small geometrical features, then the only portions of the cohesive law that need to be considered are the ones with large cohesive-length scales. Conversely, if the study is only at small geometrical scales, the larger-scale cohesive law can be neglected. Conversely, one has to be careful when measuring a cohesive law at the wrong scale if there is more than one damage / toughening mechanism operating. For example, the use of macroscopic cracks to deduce the cohesive law of composites may not provide the information needed to model crack initiation or the propagation of very small flaws. This caution is valid even if (as in the present example) all the mechanisms of interest operate during delamination, and there is no mechanism change in the initiation phase of damage.

5.2 Micro-structural features

Cohesive-length scales can also be compared to the size of micro-structural features. As will be demonstrated below, such a comparison may determine whether a higher scale of toughening mechanism can be induced by a crack jumping to a new interface and triggering large-scale bridging. LEFM models of interfacial crack propagation don't

provide any mechanism for cracks to jump between interfaces, because crack propagation will always occur from the tip of a dominant crack. Cohesive-zone models allow for such jumping provided that the strength on a neighboring interface is lowered sufficiently. While one can argue that there may be statistical variation in the strengths of neighboring interfaces, such a model only becomes realistic if the required strength fluctuations between interfaces become reasonably small relative to the local stress field. This becomes possible if the cohesive length of the interfaces is large compared to the distance between the interfaces. Large cohesive-length scales will allow crack jumping to occur with small fluctuations in cohesive strengths between neighboring interfaces. Therefore, for a given set of interface properties, crack jumping is more likely if the spacing between the interfaces is decreased. It is speculated that this may be how some biological materials derive their macroscopic toughness. Small micro-structural features, with correspondingly large cohesive-length scales, permit cracks to jump between interfaces with only limited variations in cohesive strengths, leading to a larger scale toughening by ligament-bridging between the interfaces.

Such a concept is illustrated in the simple geometry of Fig. 13. This geometry consists of a remotely-loaded edge-cracked specimen with an initial crack running along an interface. There are two secondary interfaces running parallel and at a distance h from this primary interface. Linear-hardening laws with identical cohesive-length scales were used for each interface. By varying the relative cohesive strengths of each interface, and keeping the cohesive-length scales the same, it is possible to determine the conditions under which the crack will jump to a weaker interface. This is shown in the plot of Fig. 14, which presents the maximum strength ratio between the secondary and

primary interface at which the crack jumps from the primary to secondary interface. A relatively coarse micro-structure was used, but the trend in the strength ratio required to trigger crack jumping increasing to unity as the cohesive-length scale increases is very clear. An example of a crack that has jumped to a secondary interface is given in Fig. 15. The similarity of this to observations of ligament bridging in fiber composites [Sørensen *et al.*, 2008; Sørensen, 2010] is striking, and an example of such a phenomenon from nature observed at the site of the Computational and Experimental Mechanics of Advanced Materials (CEMAM) conference is given in Fig. 16.

6. Conclusions

Damage and toughening mechanisms are two manifestations of the same process. They are both associated with a drop in the cohesive strength of an interface, and a corresponding increase in the cohesive-length scale. Any increase in the cohesive-length scale can result in crack propagation occurring at a lower level of applied stress, even with an increase in toughness. The introduction of a toughening mechanism strengthens an interface (rather than damaging it) only if it leads to a sufficiently large increase in toughness that more than compensates for the increase in cohesive-length scale. In other words, it is possible to "toughen" an interface in the sense of increasing the energy dissipation associated with crack growth, but to actually "damage" the interface in the sense of reducing the applied stress at which a crack propagates. Toughening/damage mechanisms that increase the fracture energy by more than what is required to compensate for the increase in cohesive-length scale will both strengthen and toughen the material. Merely increasing the toughness of an interface is *not* a guarantee that enhanced fracture properties will result - the effect on the cohesive-length scale

must also be considered. Since the cohesive-length scale is also dependent on the characteristic size of the material and microstructure, considerations of the efficacy of toughening mechanisms may need to take length scales into account.

The virtue of a cohesive-zone approach to fracture, over a traditional fracture-mechanics approach, is that it automatically incorporates a cohesive length that allows it to bridge all length scales. However, caution must be exercised when employing cohesive zones because fracture mechanisms are often associated with multiple length scales. A traction-separation law that doesn't capture these different scales may fail in its predictive capability when used to analyze problems at a size scale that is incompatible with the assumed cohesive length. For example, crack initiation in a composite may be associated with a mechanism (such as matrix failure) that has a much smaller cohesive length than the mechanism (such as crack bridging) associated with crack propagation. A cohesive law developed from experiments with large-scale cracks, and with a correspondingly large cohesive-length scale, may not be appropriate at the smaller length scales associated with crack initiation. If there are multiple mechanisms for crack propagation, the cohesive law must be developed at the scale(s) of interest. Conversely, there is no need to develop cohesive laws for failure mechanisms with cohesive lengths outside the scale of practical interest.

One important role of cohesive-length scales is their effect on describing the extent to which fracture may be delocalized. If there are micro-structural features that are significantly smaller than the cohesive length, then the conditions for failure may not be localized on the plane ahead of a macroscopic crack. This can induce crack jumping to neighboring interfaces, creating distributed damage and bridging ligaments. These, in

turn, can introduce toughening at larger length scales, possibly creating hierarchical toughening mechanisms.

Acknowledgements

MDT was partially supported by the Department of Energy under Award Number DE-PI0000012, through the Clean Energy Research Center—Clean Vehicle Consortium. MDT also acknowledges support from the Øtto Mansted fund for a visit to the Danish Technical University. Sandia National Laboratories is a multi-program laboratory managed and operated by Sandia Corporation, a wholly owned subsidiary of Lockheed Martin Corporation, for the U.S. Department of Energy's National Nuclear Security Administration under contract DE-AC04-94AL85000.

References

Bao, G. and Suo, Z. (1992). "Remarks on Crack-Bridging Concepts," *Applied Mechanics Review*, **45**, 355-366.

Cox, B. N. and Marshall, D. B. (1994). "Concepts for Bridged Cracks in Fracture and Fatigue," *Acta Metallurgica et Materialia*, **42**, 341-364.

Hillerborg, A., Modéer, M., and Petersson, P. E. (1976). "Analysis of Crack Formation and Crack Growth in Concrete by Means of Fracture Mechanics and Finite Elements," *Cement and Concrete Research*, **6**, 773-782.

Li, S., Thouless, M. D., Waas, A. M., Schroeder, J. A. and Zavattieri, P. D. (2005). "Use of a Cohesive-Zone Model to Analyze the Fracture of a Fiber-Reinforced Polymer-Matrix Composite," *Journal of Composites Science & Technology*, **65**, 537-549.

Ritchie, R. O. (2011). "The Conflicts between Strength and Toughness," *Nature Materials*, **10**, 817-822.

Sills, R. B. and Thouless, M. D. (2013). "The Effect of Cohesive-Law Parameters on Mixed-Mode Fracture," *Engineering Fracture Mechanics*, **109**, 353-368.

Sørensen, B. F. and Jacobsen, T. K. (1998). "Large-Scale Bridging in Composites: *R*-Curves and Bridging Laws," *Composites,* **29A**, 1443–1451.

Sørensen, B. F. and Jacobsen, T. K. (2009). "Characterizing Delamination of Fibre Composites by Mixed Mode Cohesive Laws," *Composites Science and Technology,* **69**, 445–456.

Sørensen, B. F., Gamstedt, E. K., Østergaard, R. C. and Goutianos, S. (2008). "Micromechanical Model of Cross-over Fibre Bridging," *Mechanics of Materials,* **40**, 220-234.

Sørensen, B. F. (2010). "Cohesive Laws for Assessment of Materials Failure: Theory, Experimental Methods and Application," Doctor of Technices Thesis, Danish Technical University, Lyngby, Denmark.

Tada H., Paris P. C., Irwin G. R. (1985). "The Stress Analysis of Cracks Handbook," 2nd edition. Paris Productions Inc. St. Louis, MO, USA.

Thouless, M. D. (1988). "Bridging and Damage Zones in Crack Growth," *Journal of the American Ceramic Society*, **71**, 408-413.

Yang, Q. D., Thouless, M. D. and Ward, S. M. (1999). "Numerical Simulations of Adhesively-Bonded Beams Failing with Extensive Plastic Deformation," *Journal of the Mechanics and Physics of Solids*, **47**, 1337-1353.

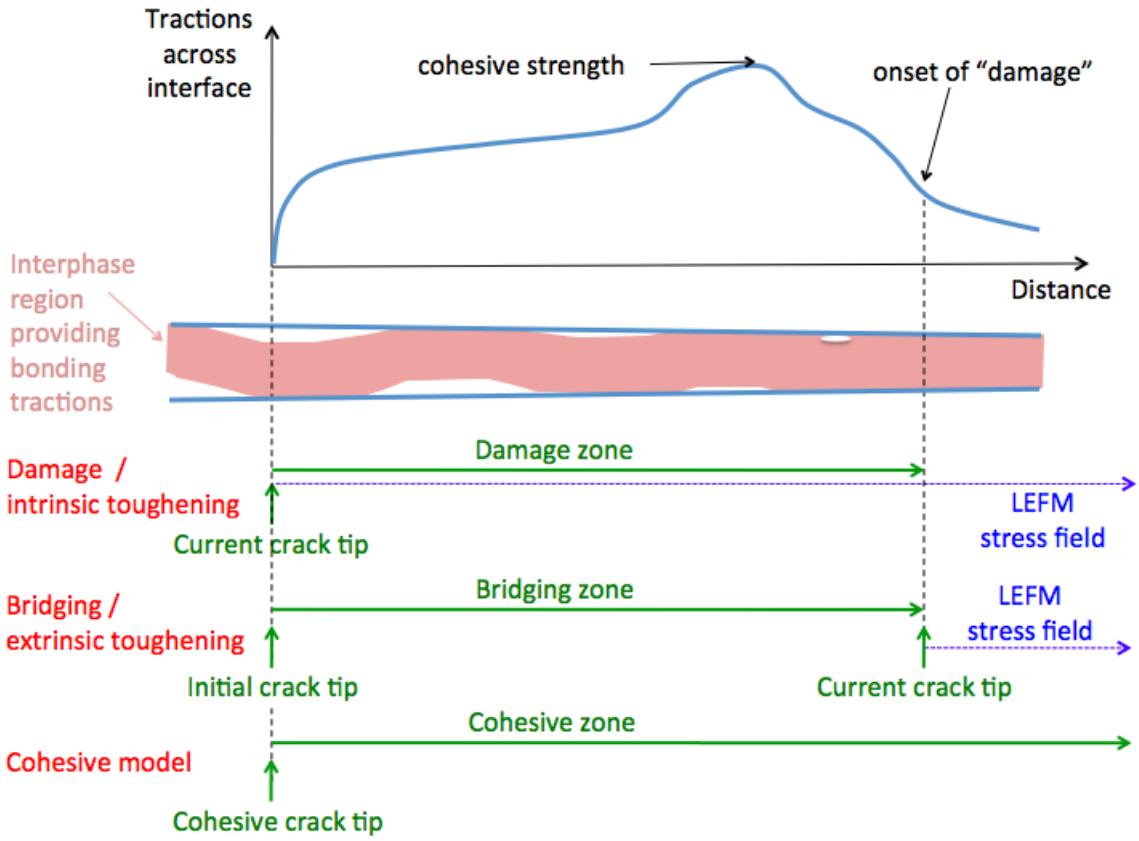

Figure 1 Comparisons between the assumed locations of crack tips for extrinsic toughening models, intrinsic toughening models and cohesive-zone models. All these represent the same physical reality..

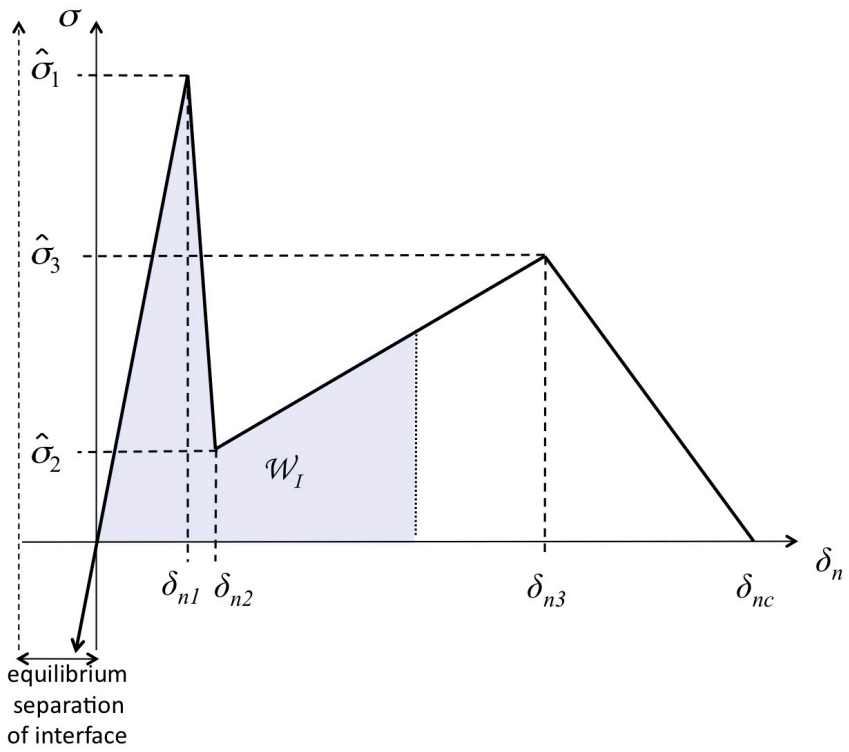

Figure 2: Generic mode-I traction-separation law. It should be emphasized that the origin of cohesive tractions and displacements should always occur at the equilibrium separation of the interface; this allows for some compressive contributions to the mode-I traction-separation law.

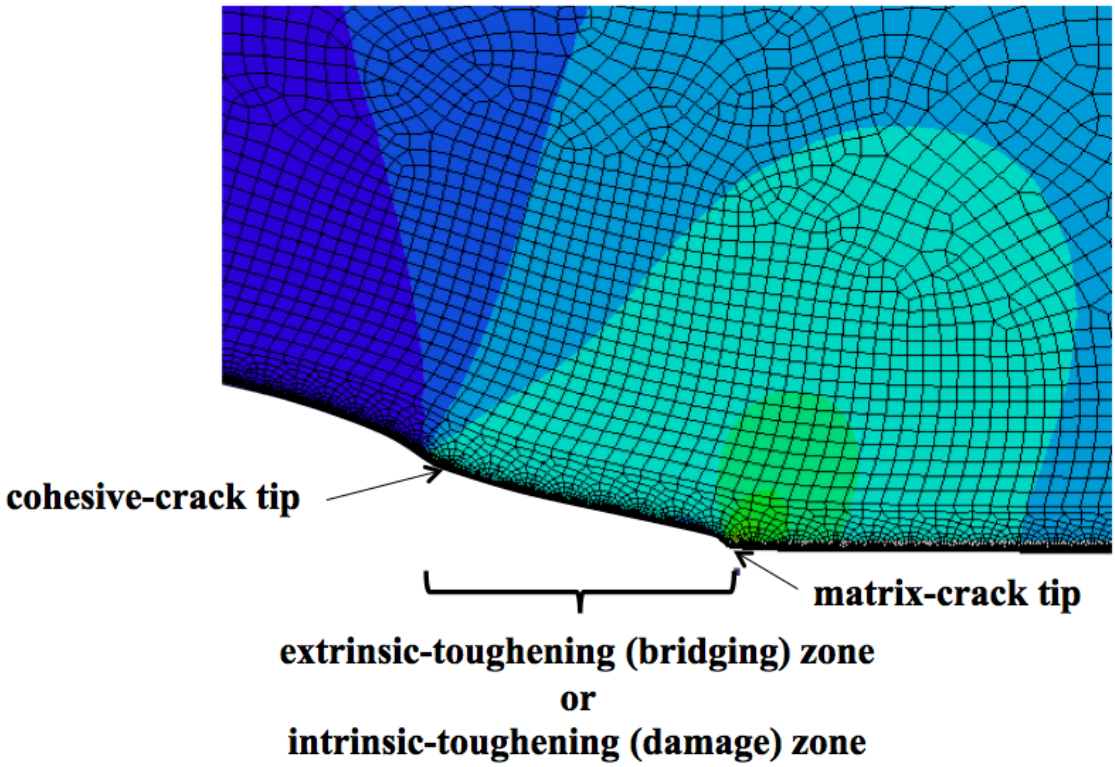

Figure 3: Mesh at crack tip showing the deformation at different regions of the cohesive law. The region between the cohesive-crack tip and the matrix-crack tip is considered to be an extrinsic-toughening or bridging zone from the perspective of the matrix-crack tip. It is considered to be an intrinsic-toughening or damage zone from the perspective of the cohesive-crack tip. Contours show the normal stresses orthogonal to the crack plane.

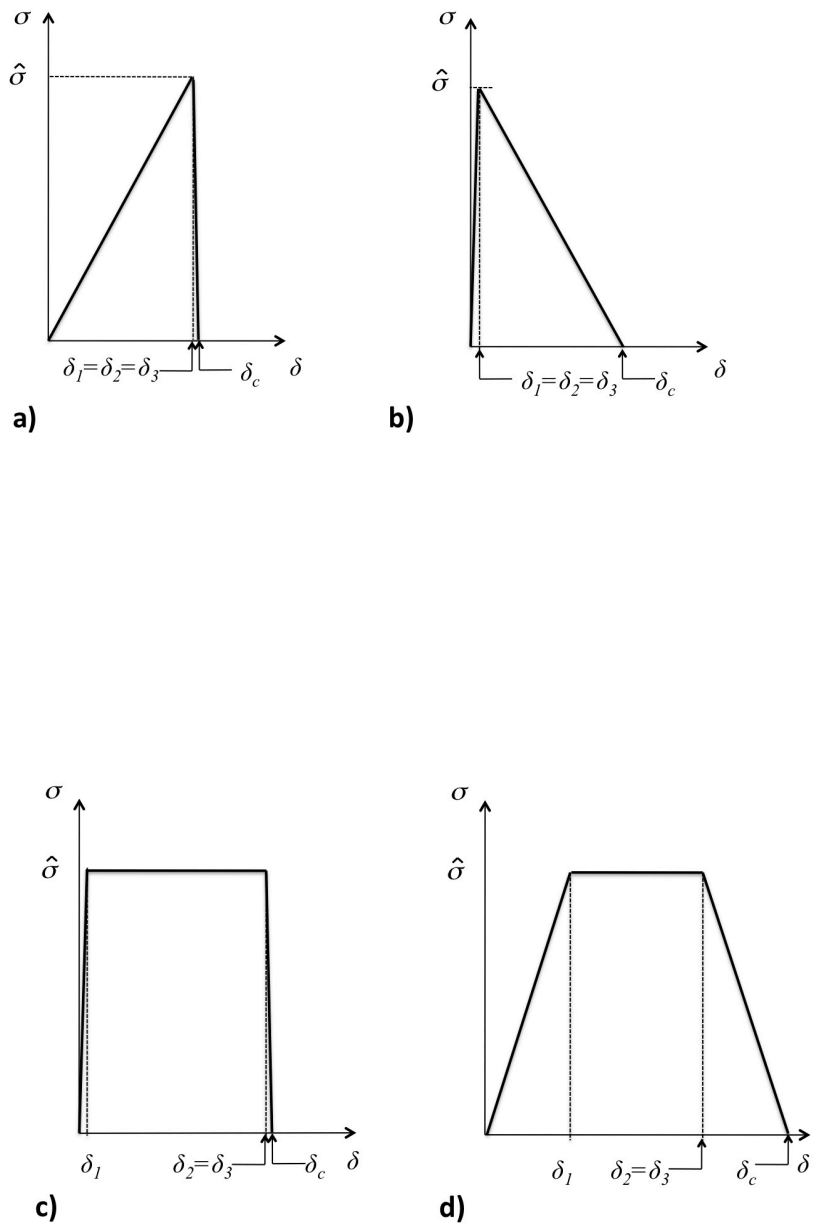

Figure 4 Examples of simple cohesive-laws: **(a)** linear-hardening case with no damage; **(b)** linear-softening; **c)** constant-stress; **(d)** trapezoidal.

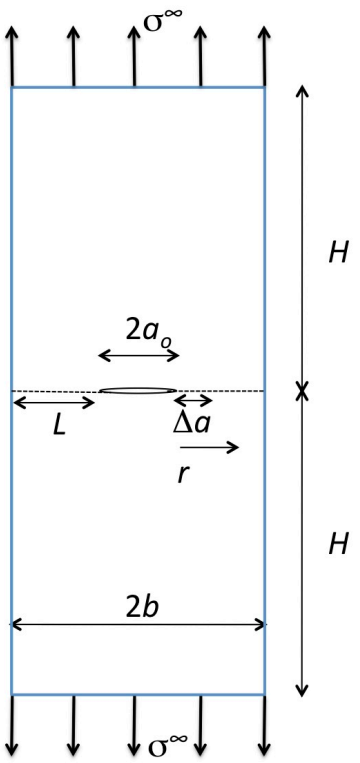

Figure 5 Center-cracked geometry used for the analysis.

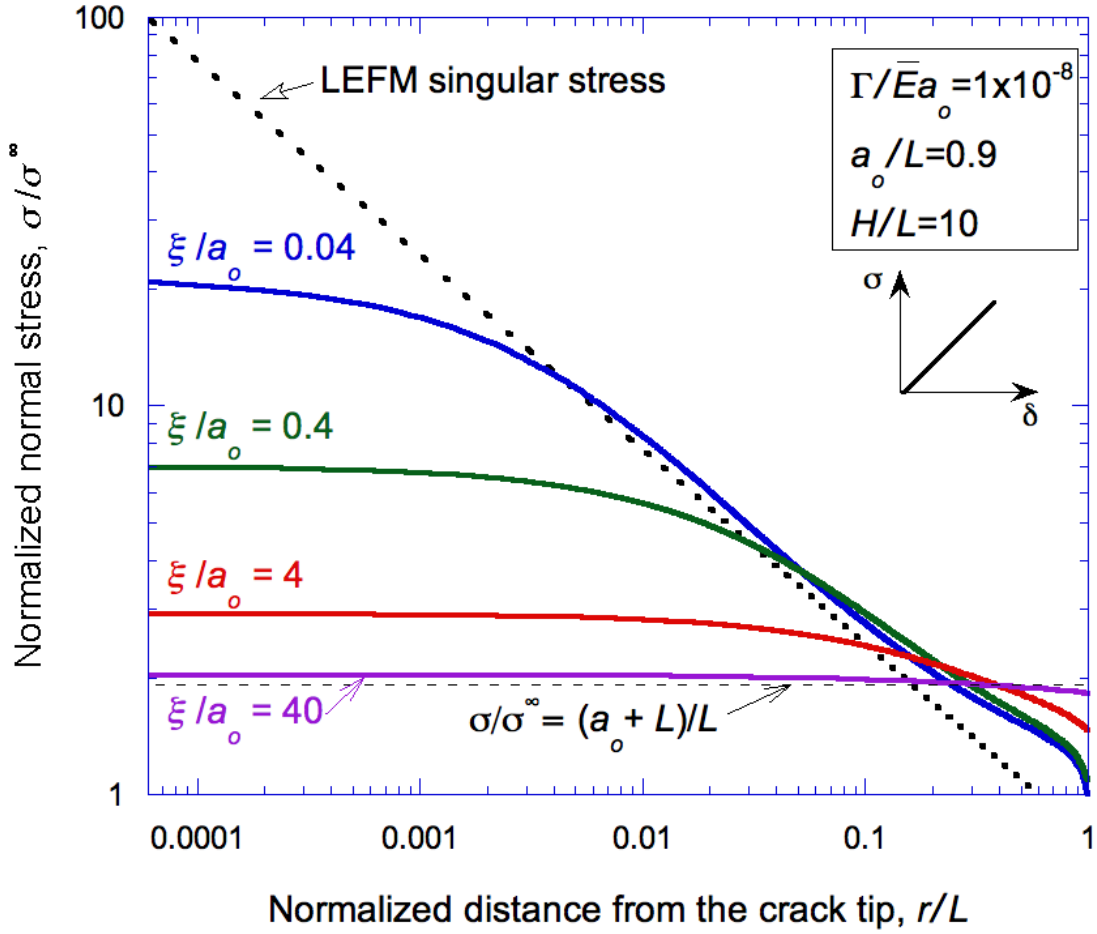

Figure 6 Stress field ahead of crack for different linear-hardening laws. Note that, since the instantaneous cohesive length is fixed for a linear-hardening law, the normalized stress fields do not change during loading. At very large values of the instantaneous cohesive-length scale, the stress tends to a uniform value along the interface. For a linear-hardening law, the cohesive-length is constant, so $\xi = \xi_o$.

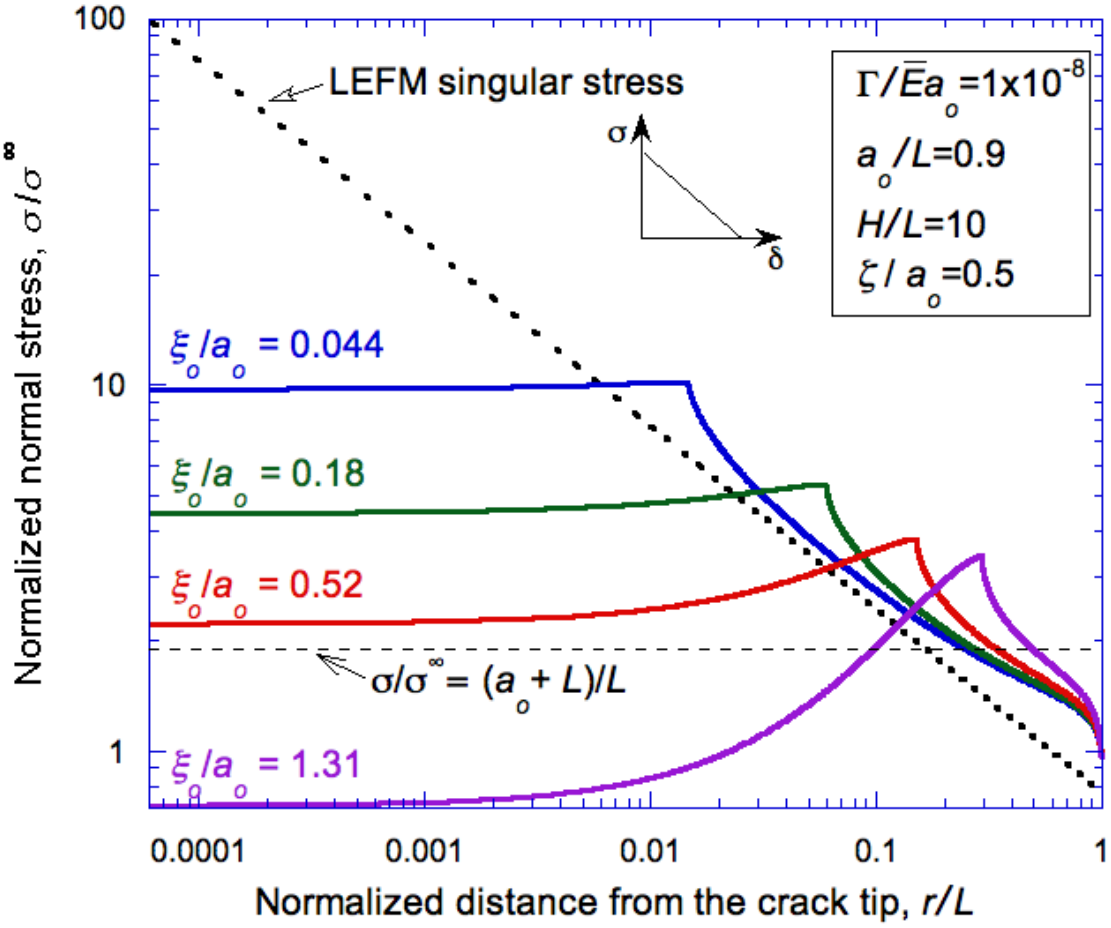

Figure 7(a) Evolution of the stress field ahead of the cohesive-crack tip during loading for a linear-softening law with a nominal fracture-length scale of $\zeta/a_o = 5$. As the remote stress, σ^{∞}, increases, the instantaneous cohesive length at the crack tip, ξ_o, also increases. Plots corresponding to various values of the crack-tip instantaneous cohesive-length scale ξ_o/a_o are shown.

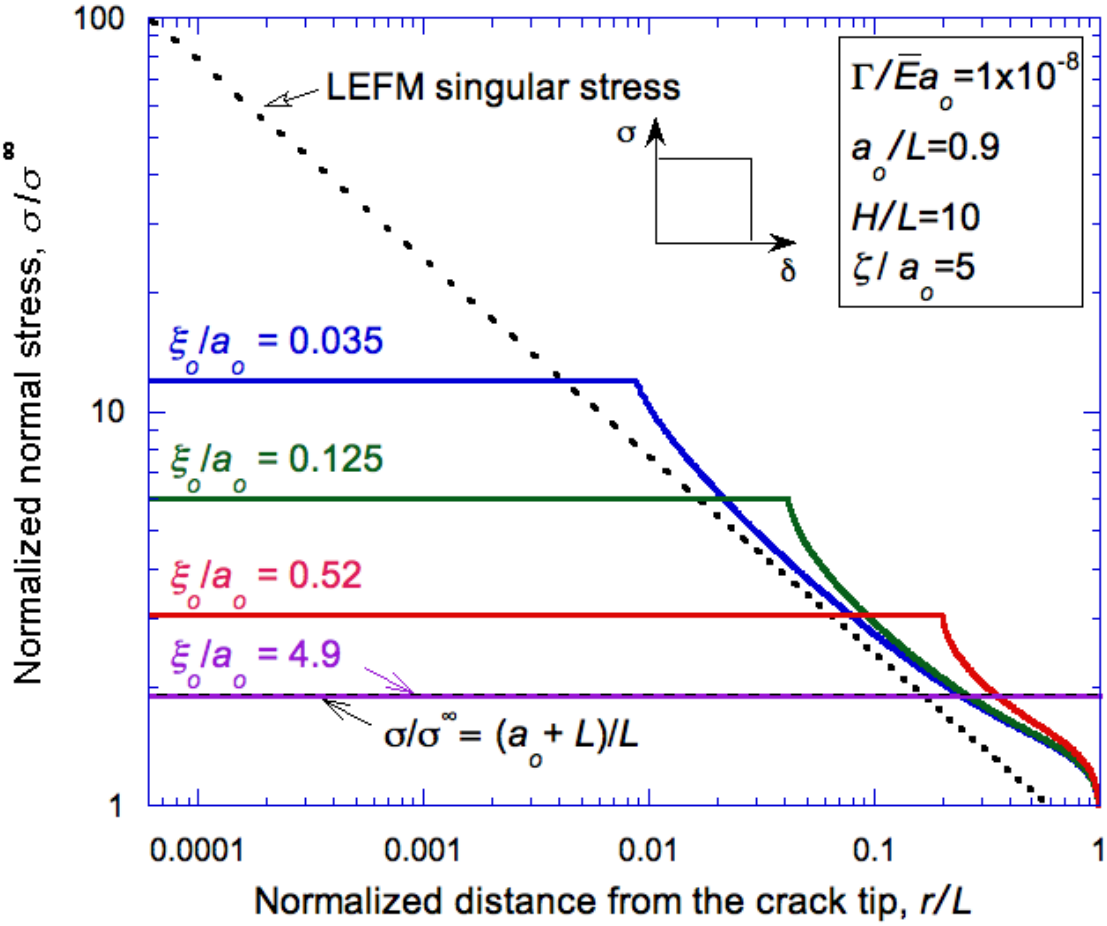

Figure 7(b) Evolution of the stress field ahead of the cohesive-crack tip during loading for a constant-stress law with a nominal fracture-length scale of $\zeta/a_o = 5$. As the remote stress, σ^{∞}, increases, the instantaneous cohesive length at the crack tip, ξ_o, also increases. Plots corresponding to various values of the crack-tip instantaneous cohesive-length scale ξ_o/a_o are shown.

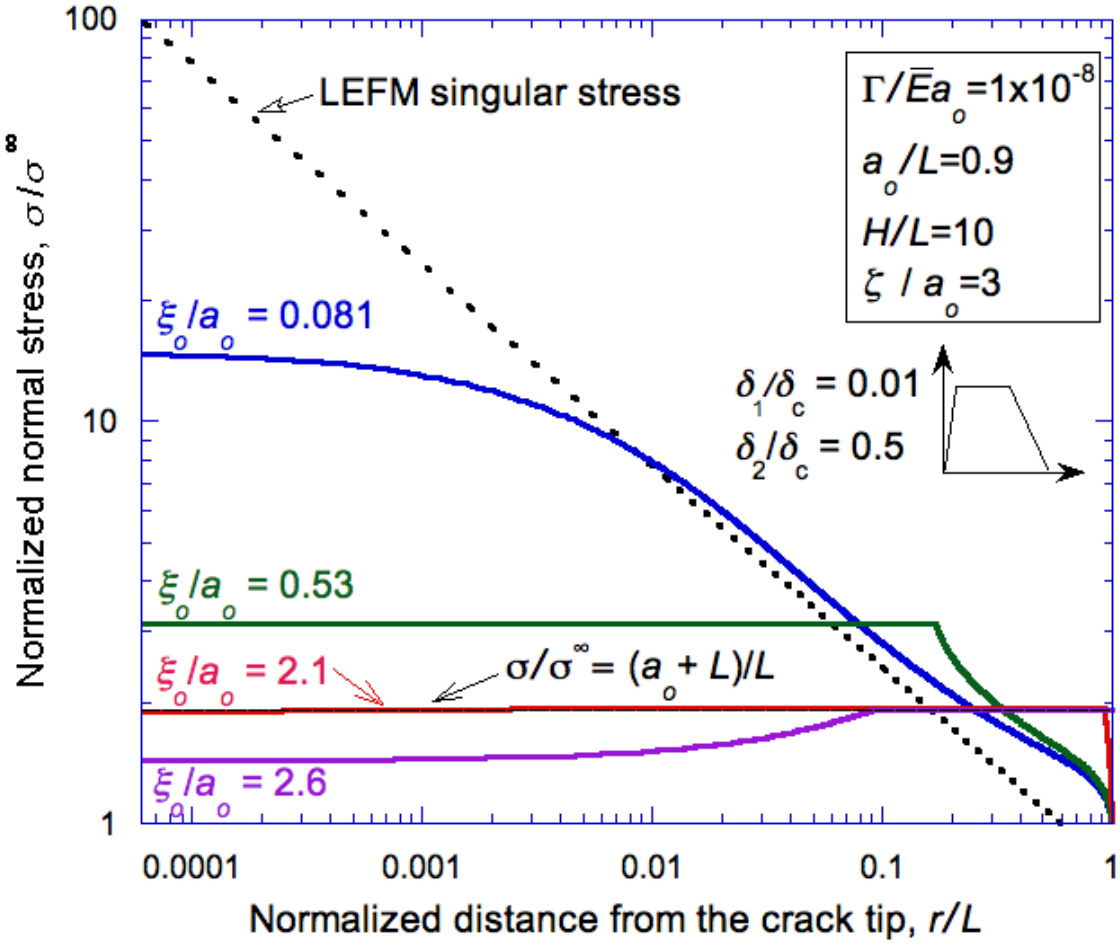

Figure 7(c) Evolution of the stress field ahead of the cohesive-crack tip during loading for a trapezoidal law with a nominal fracture-length scale of $\zeta/a_o = 3$. As the remote stress, σ^{∞}, increases, the instantaneous cohesive length at the crack tip, ξ_o, also increases. Plots corresponding to various values of the crack-tip instantaneous cohesive-length scale ξ_o/a_o are shown.

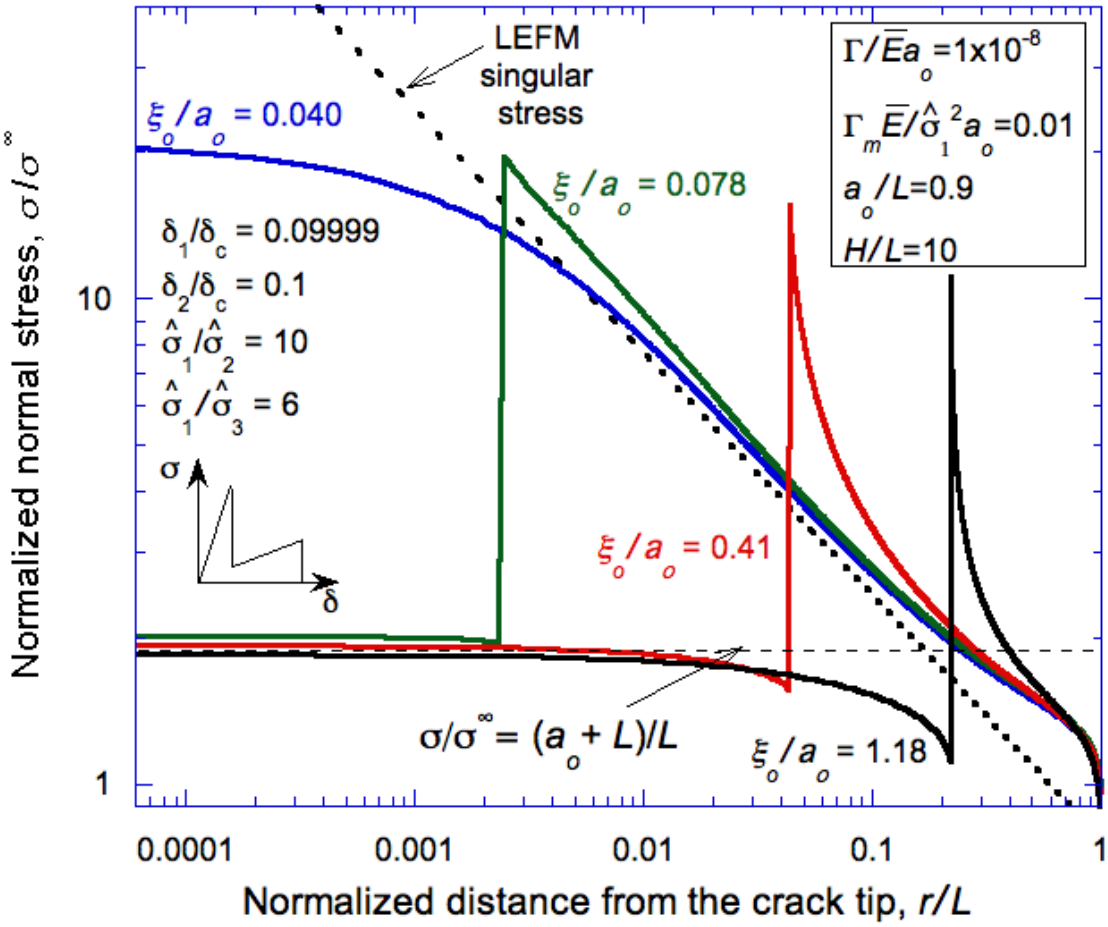

Figure 7(d) Stress field ahead of the cohesive crack tip for a cohesive law representing a fiber composite, from the initial loading of the unbridged matrix crack (for which ξ_o/a_o = 0.040) until the crack is fully bridged (ξ_o/a_o = 1.18). The nominal fracture length scale for this law is ζ/a_o = 3.4, based on $\hat{\sigma}_1$.

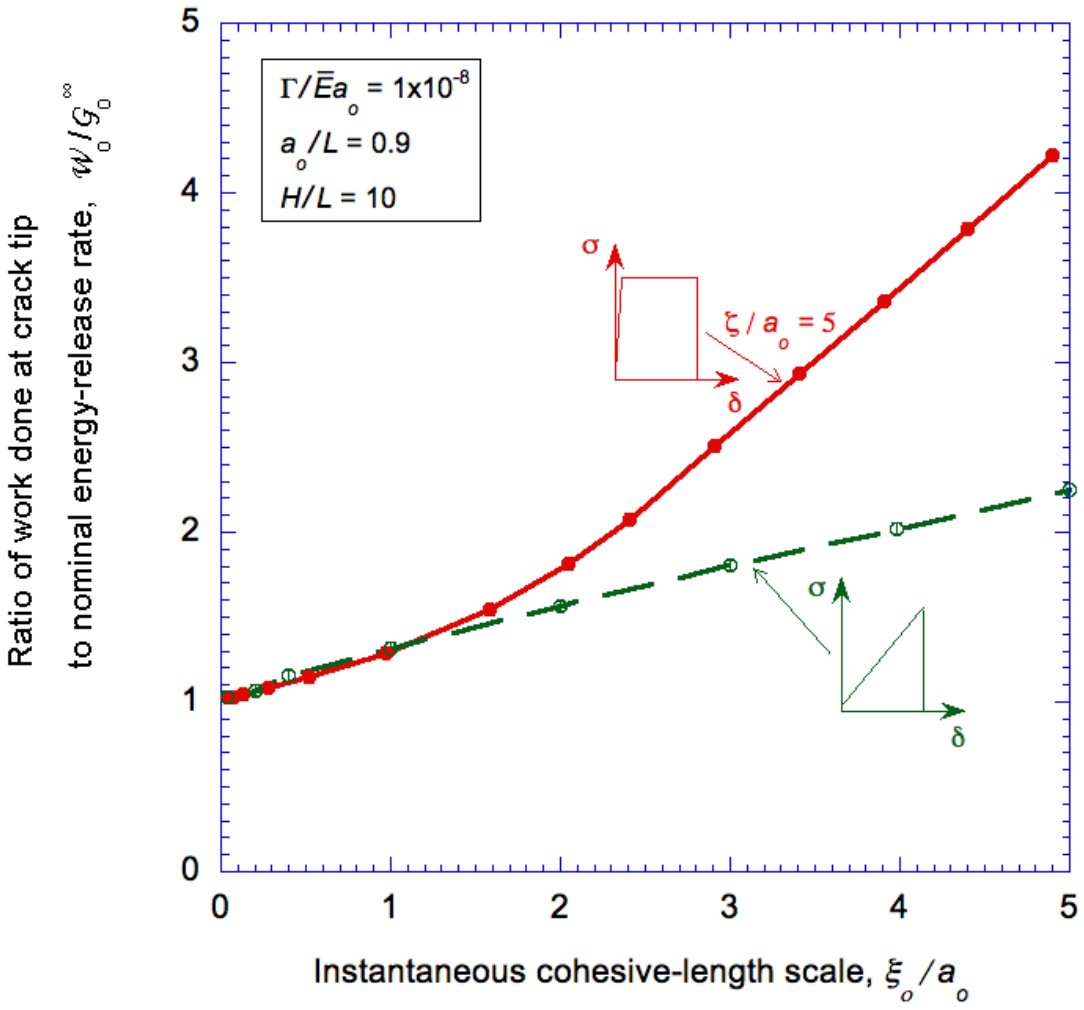

Figure 8(a) Evolution of the ratio of the work done by the crack-tip tractions to the nominal energy-release rate calculated from LEFM, using a constant-stress and linear-hardening cohesive law. The relative increase in $\mathcal{W}_o$ is associated with the additional compliance from the cohesive zone ahead of the crack tip. It results in a failure load that is lower than that predicted by LEFM.

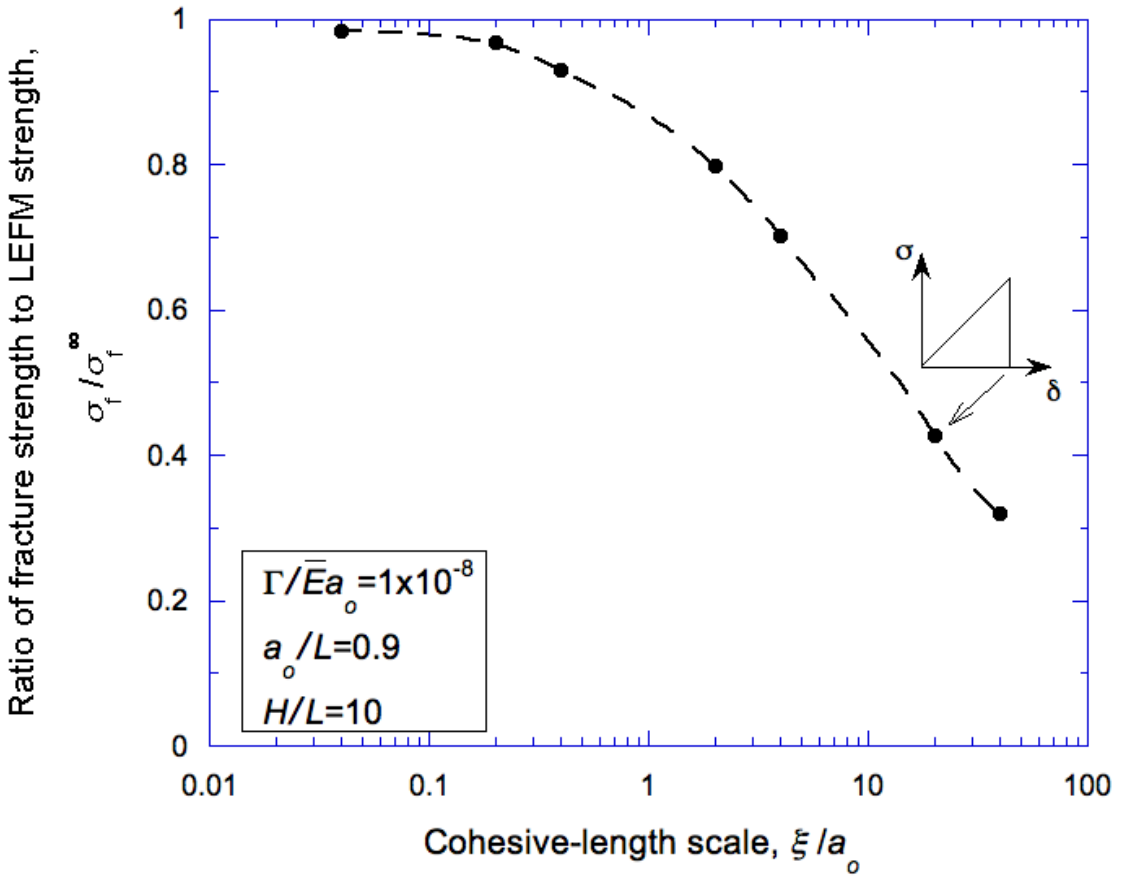

Figure 8(b) An increase in the cohesive-length scale decreases the fracture strength of a cracked body. As the cohesive-length scale decreases to zero, the strength asymptotes to the strength predicted by LEFM (toughness-controlled strength). As the cohesive-length scale increases, the strength tends to the cohesive-strength controlled limit.

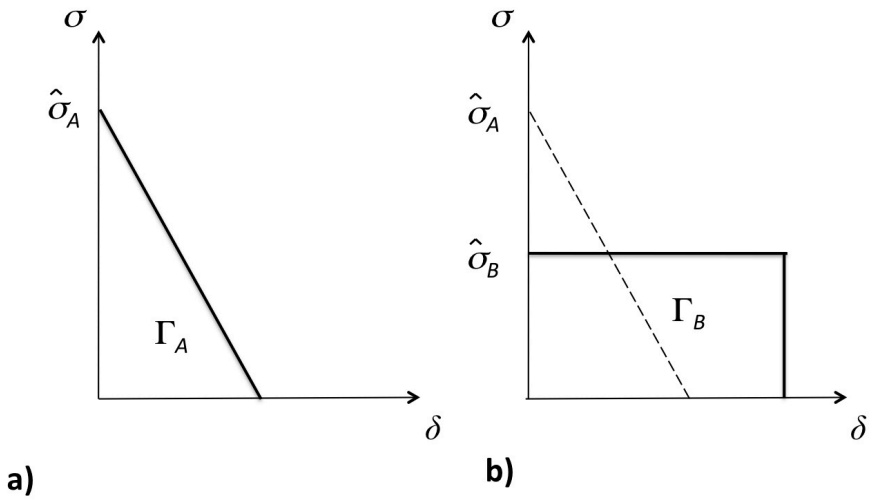

Figure 9 Introducing a new toughening mechanism triggered by dropping the cohesive strength from $\hat{\sigma}_A$ to $\hat{\sigma}_B$ may not result in a stronger material, even if the new toughness, Γ_B, is greater than the original toughness, Γ_A. This is because the cohesive-length scale at fracture for mechanism "B" will be larger than for mechanism "A".

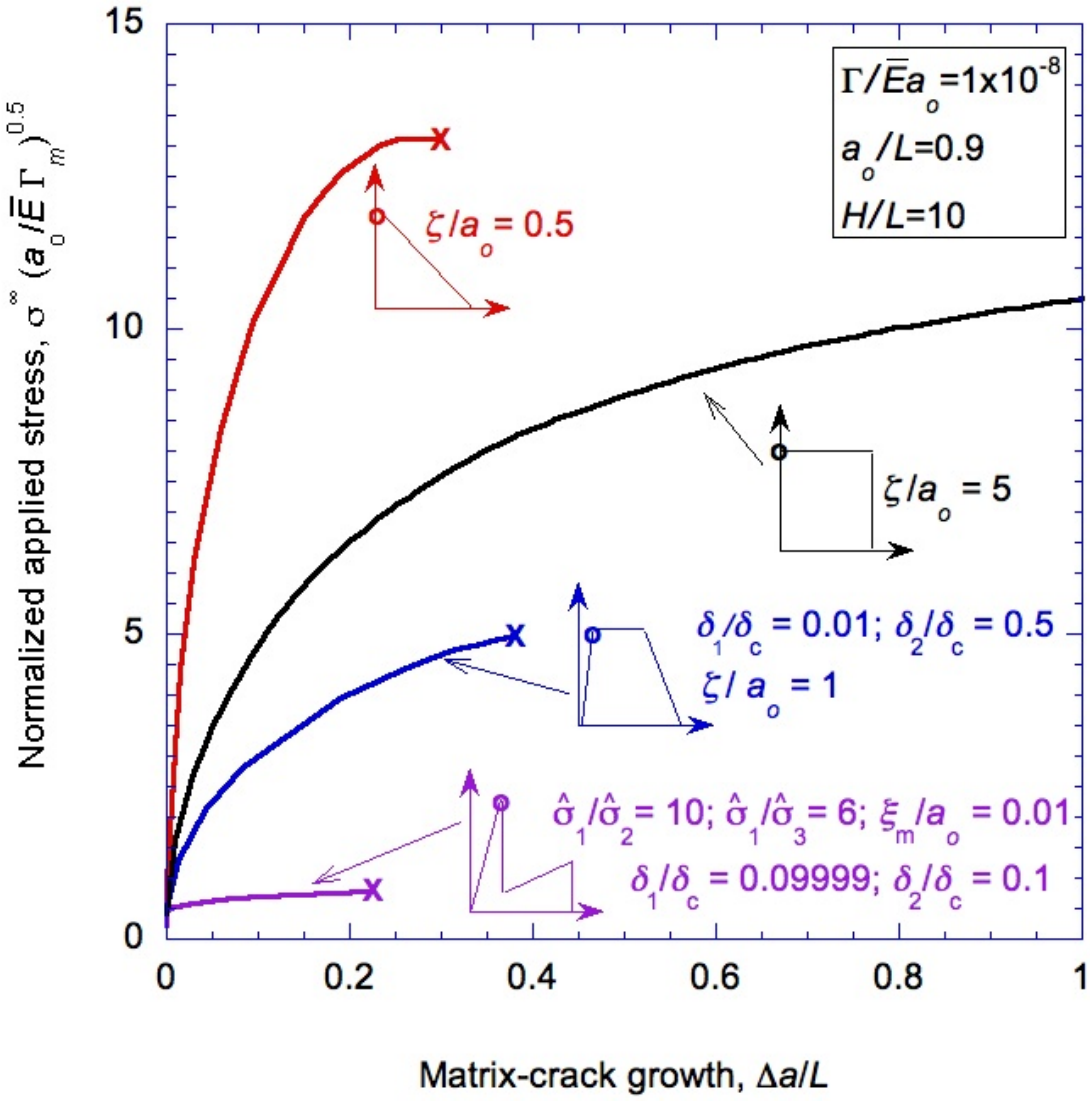

Figure 10(a) Applied stress as a function of the matrix crack growth for various cohesive laws. The "o" on the cohesive curve represents the onset of matrix cracking. An "X" on a plot marks the onset of a fracture instability; this occurred at $\delta/\delta_c = 1$ for the fiber-bridging law, $\delta/\delta_c = 0.792$ for the linear-softening law, and $\delta/\delta_c = 0.827$ for the trapezoidal law.

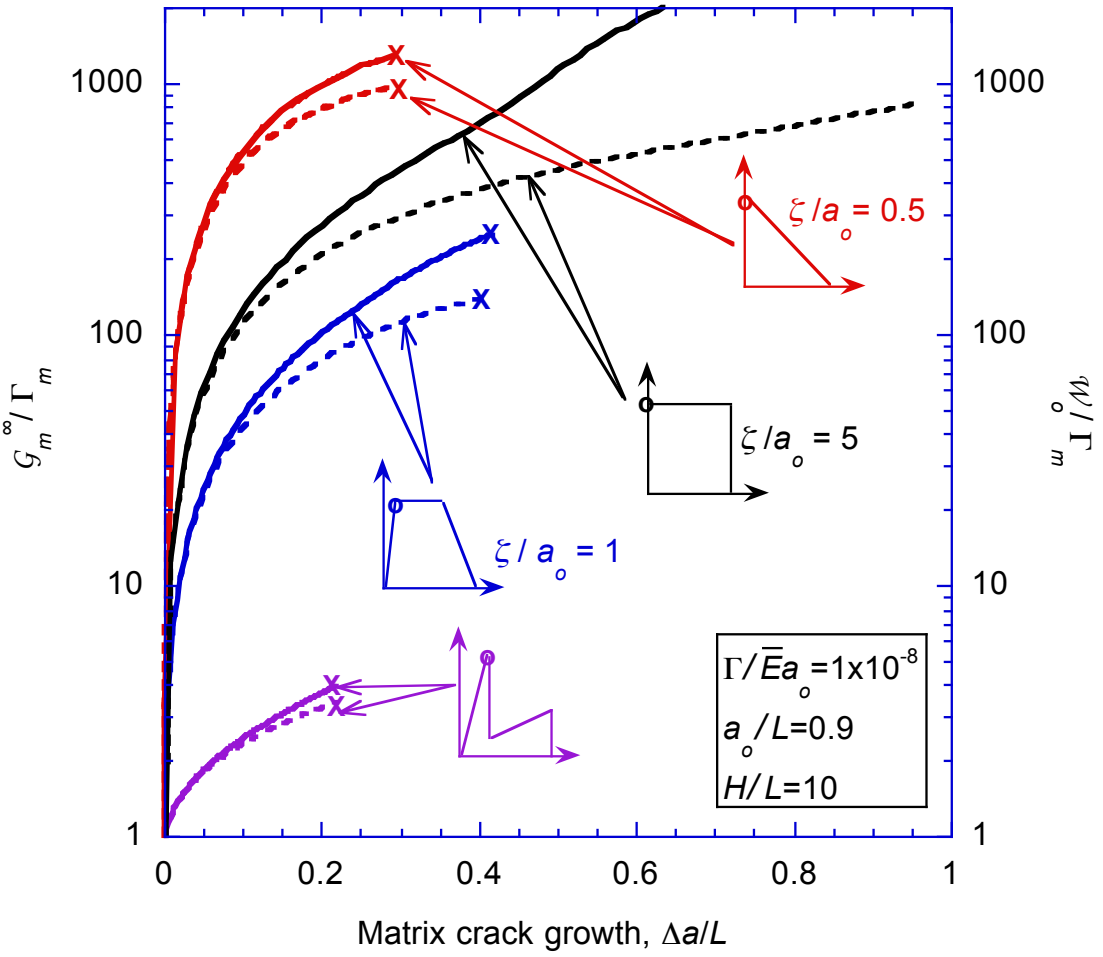

Figure 10(b) *R*-curves calculated from the data of Fig. 10a. The "o" on the cohesive curve represents the onset of matrix cracking. An "X" on a plot marks the onset of a fracture instability. These plots (solid lines) show $\mathcal{G}_m^\infty/\Gamma_m$ plotted against crack growth, where $\mathcal{G}_m^\infty$ is defined in terms of the matrix crack length and the applied stress. A comparison is also made between these curves and $\mathcal{W}_o/\Gamma_m$ (dashed lines).

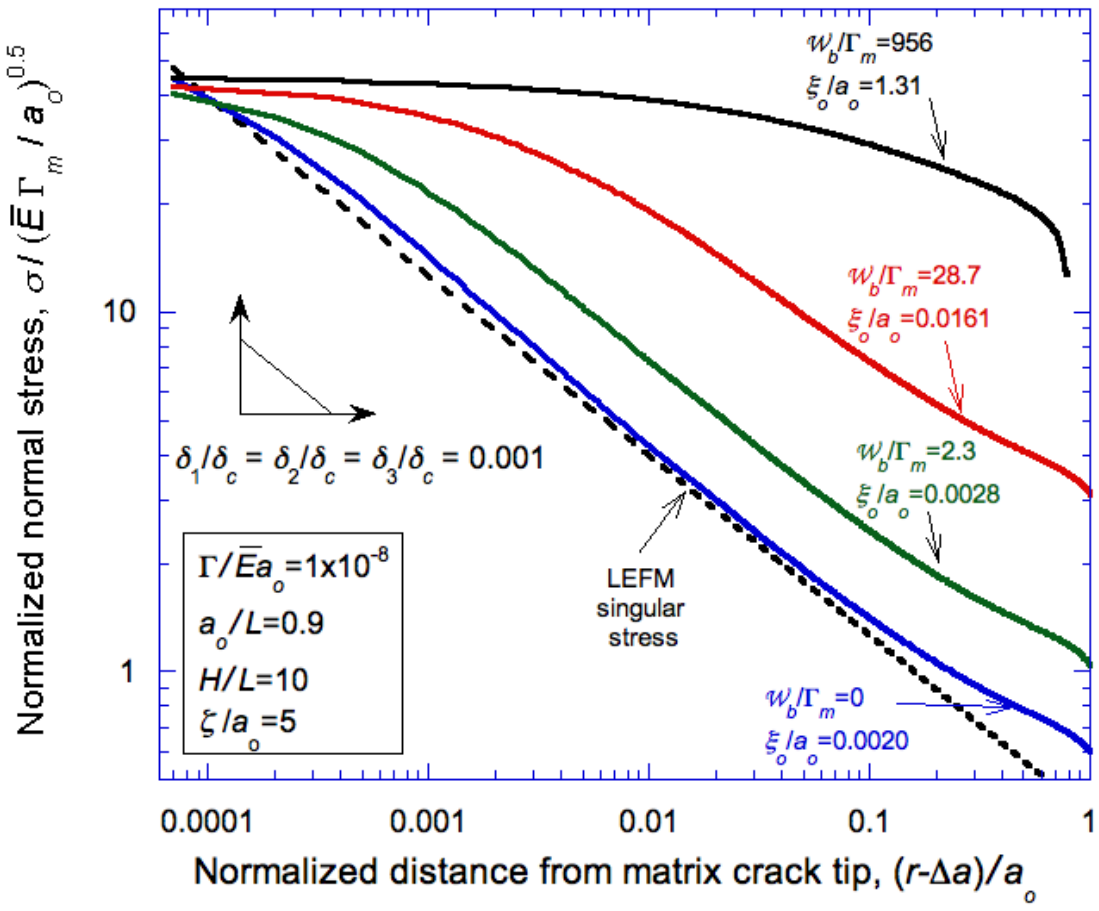

Figure 11(a) Stress ahead of the matrix crack tip at the condition for matrix crack growth for a linear-softening cohesive law.

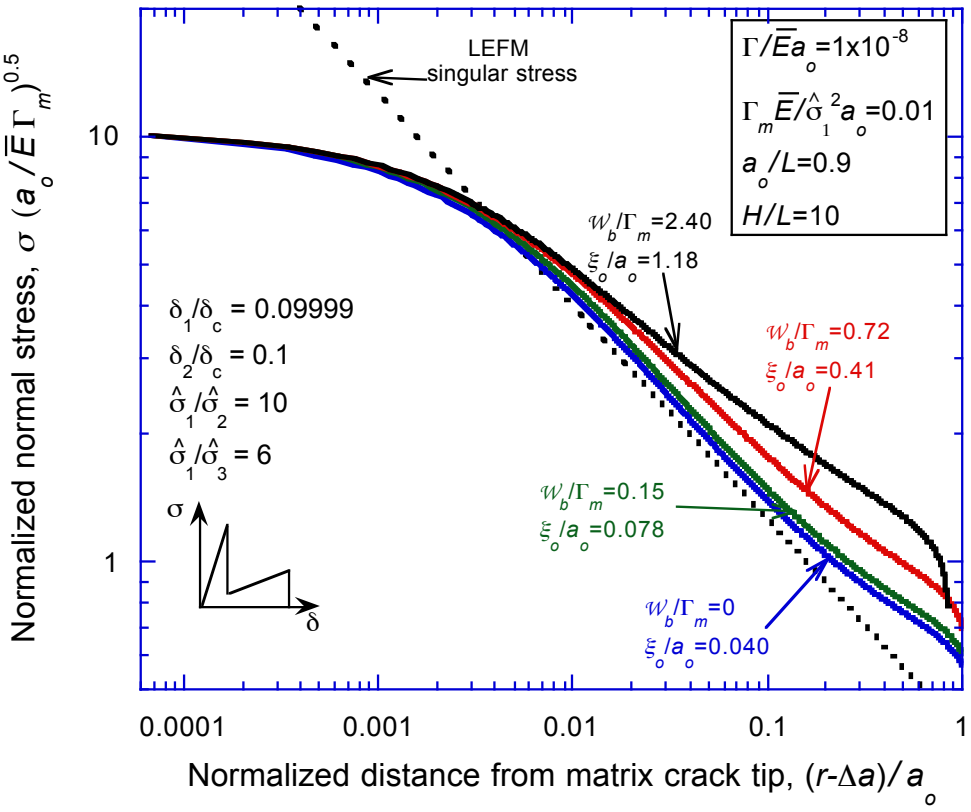

Figure 11(b) Stress ahead of the matrix crack tip at the condition for matrix crack growth for a cohesive law representing a fiber composite, from the initial growth of the unbridged crack ($\mathcal{W}_b/\Gamma_m$ = 0), until the crack is fully bridged ($\mathcal{W}_b/\Gamma_m$ = 2.40).

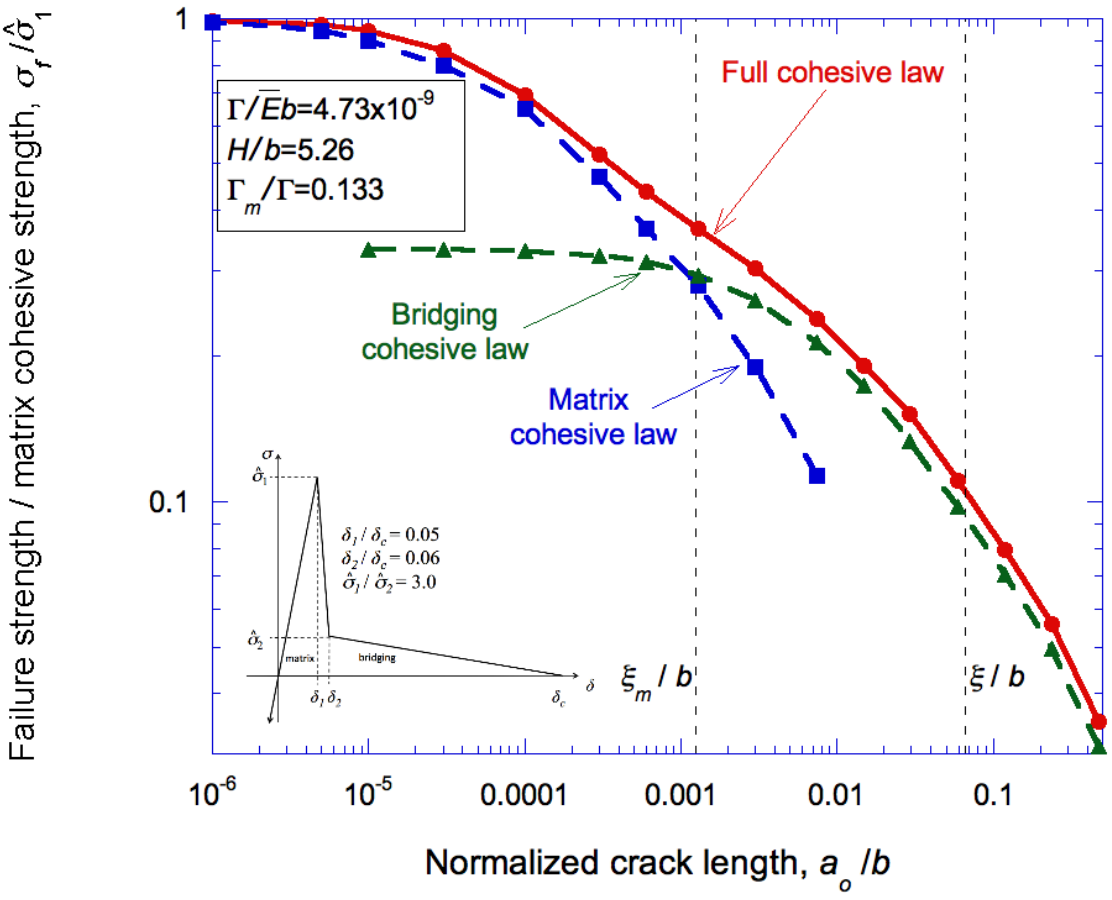

Figure 12 Predictions for failure strength of a crack with a cohesive law representing fiber-bridging in a composite. A comparison is made between the predictions for the full law, with predictions made assuming only the matrix portion of the law, and predictions made assuming only the bridging portion of the law.

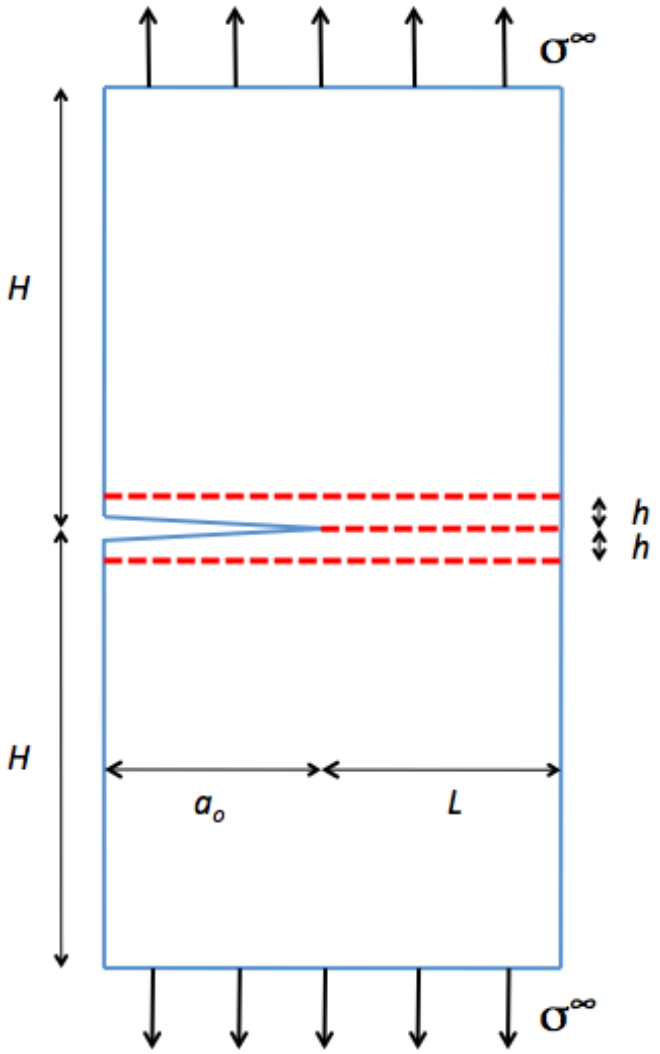

Figure 13 Geometry for investigating crack jumping across interfaces. Linear-hardening laws with the same cohesive-length scale were used for all interfaces, but different cohesive strengths were assigned to different interfaces. The dashed red lines correspond to the interfaces along which there are cohesive zones.

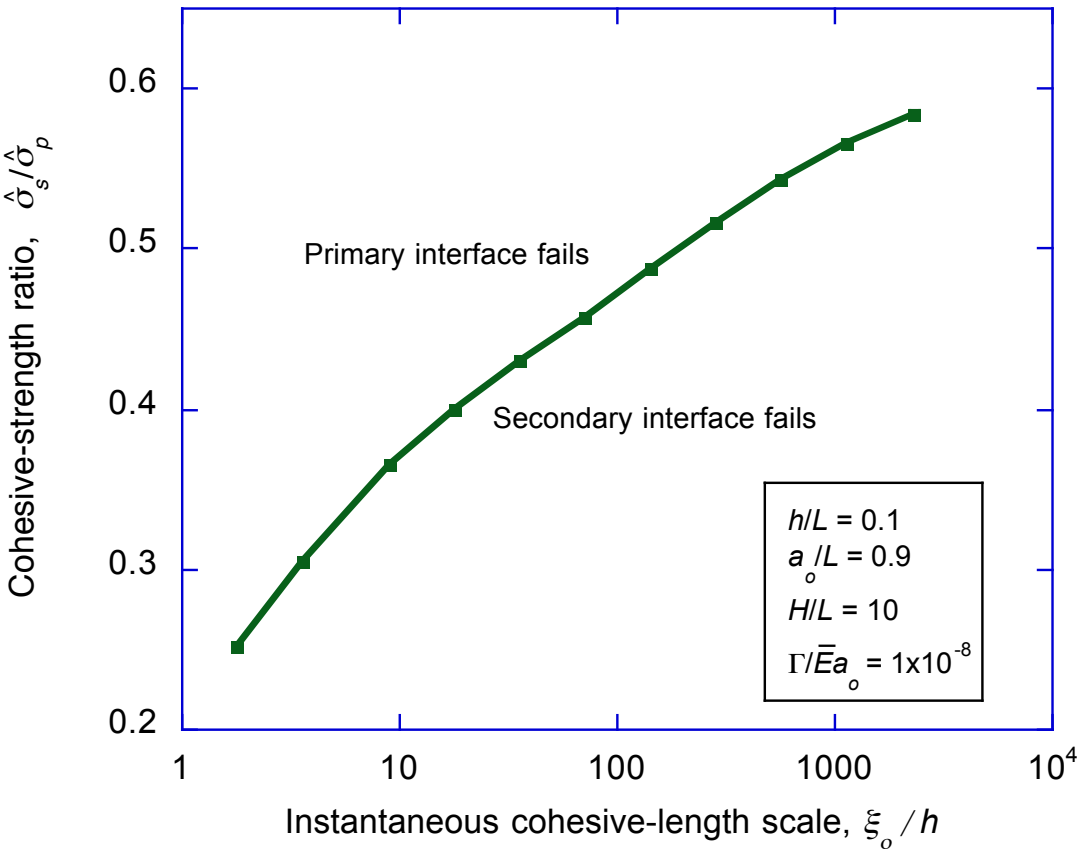

Figure 14 A plot of the critical ratio for the cohesive strength of the secondary interface to the cohesive strength of the primary interface required for crack jumping, as a function of the cohesive-length scale used for all three interfaces. All the interfaces have linear-hardening laws, which are identical in mode-I and mode-II.

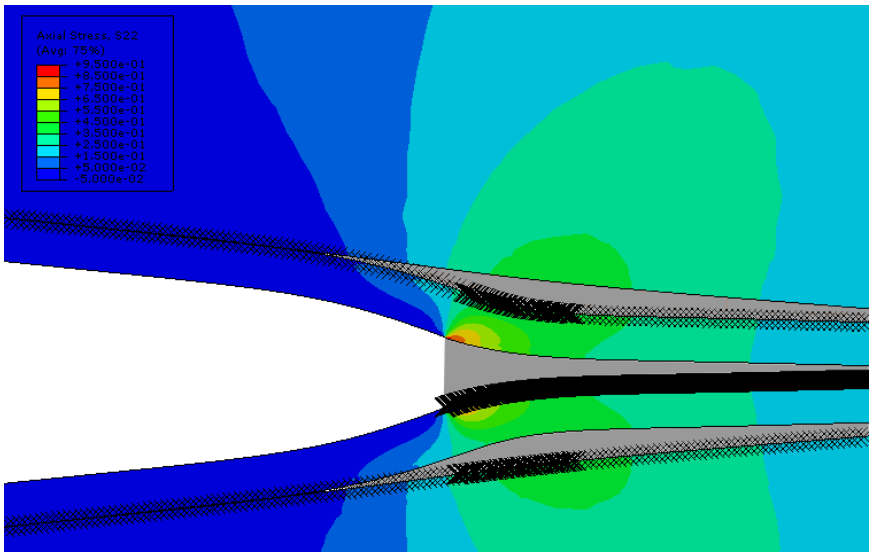

(a)

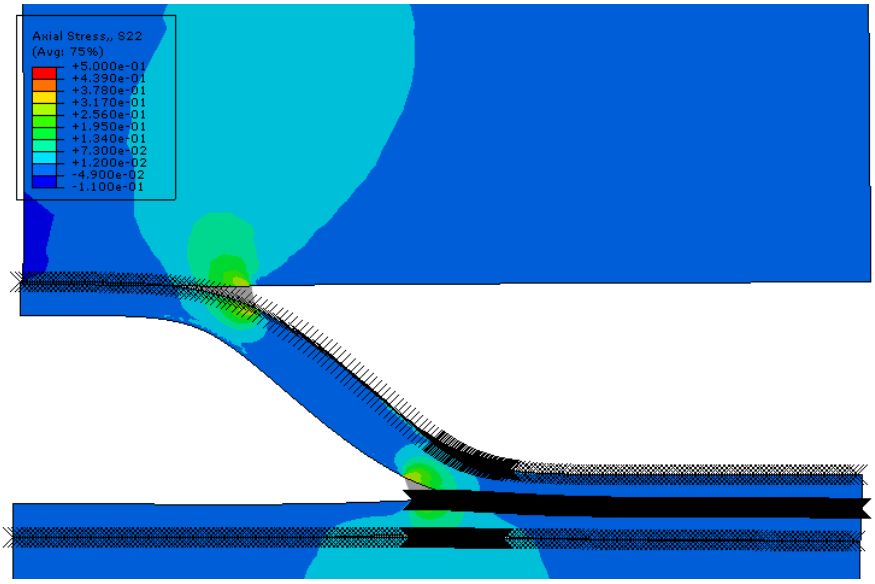

(b)

Figure 15 **(a)** Deformation of the cohesive zones near the original crack tip for the geometry shown in Fig. 13 just before crack growth. **(b)** Delamination after the crack has jumped from the primary interface to the secondary interface. For these figures, the bottom secondary interface was given the same cohesive strength as the primary interface, so the crack could only jump to the top interface. In both of these figures, an "X" indicates the location of cohesive elements, and the grey areas represent regions where the tractions are still acting. All interfaces have linear-hardening laws with $\xi_o/h = 9$; the cohesive strength of the top secondary interface is 40% of the cohesive strength of the primary interface. The stress contours are normal stresses orthogonal to the crack plane normalized by the cohesive strength of the primary interface.

Figure 16 Crack jumping across interfaces exhibited in a natural composite (the bark of a coconut tree) observed at the marina in KAUST (site of the CEMAM 2013 conference).